Japanese Journal of Gastroenterology and Hepatology

Research Article

ISSN: 2435-1210 | Volume 10

A Novel Mitophagy Related Lncrna Signature for Predicting Prognosis in Gastric Adenocarcinoma

Mengyu Hao[1#], Jiahao Guan[1#], Yuetong Huang[2] and Guizhen Pan[1*]

[1]Department of Radiotherapy, the First Affiliated Hospital, Anhui Medical University, Hefei, PR China

[2]Department of Gastrointestinal and Gland Surgery, The First Affiliated Hospital of Guangxi Medical University, Nanning 530021, China

***Corresponding author:**

Guizhen Pan,
Department of Radiotherapy, the First Affiliated Hospital, Anhui Medical University, Hefei, PR China

Received: 02 Jan 2025
Accepted: 10 Jan 2025
Published: 21 Jan 2025
J Short Name: JJGH

Citation:

Guizhen Pan. A Novel Mitophagy Related Lncrna Signature for Predicting Prognosis in Gastric Adenocarcinoma. J Gastro Hepato. 2025; V10(14): 1-16

Keywords:

Mitophagy; Gastric Cancer; Long Non-Coding RNA; Risk Signature; Tumor Microenvironment; Bioinformatics

Abbreviations:

STAD: Gastric Adenocarcinoma; TCGA: The Cancer Genome Atlas; MRGs: Mitophagy Related Genes; MRlncRNAs: Mitophagy Related lncRNAs; DElncRNAs: Differentially Expressed lncRNAs; LASSO: The Least Absolute Shrinkage and Selection Operator; OS: Overall Survival; ROC: Time-Dependent Receiver Operating Characteristic; C-index: Concordance Index; PCA: Principal Component Analysis; GO: Gene Ontology; KEGG: Kyoto Encyclopedia of Genes and Genomes; TMB: Tumor Mutation Burden

1. Abstract

1.1. Aim

This study aimed to develop a predictive signature based on mitophagy-related lncRNAs to assess their prognostic and immunological significance in STAD patients.

1.2. Methods

Based on the STAD transcriptome data and clinical profiles from The Cancer Genome Atlas (TCGA), we identified mitophagy-related lncRNAs through co-expression and differential analyses. The least absolute shrinkage and selection operator (LASSO) algorithm combined with Cox regression was then used to constructed a risk signature, and then categorized patients into high- and low-risk groups. Prognostic performance of the signature was evaluated by employing Kaplan-Meier survival analysis, receiver operating characteristic (ROC) curve analysis, independent prognostic analysis. Additionally, KEGG, GO, and GSEA analyses were used to elucidate the biological functions associated with the risk signature. Finally, the tumor microenvironment, drug sensitivity, and tumor mutational burden (TMB) in relation to this signature were also investigated.

1.3. Result

A signature comprised 9 mitophagy-related lncRNAs was constructed. Kaplan-Meier analysis revealed that patients with high-risk group had a poor overall survival. Cox regression and ROC analyses affirmed the robust predictive performance of the signature. Immunological profiling revealed increased immune cell infiltration and immune checkpoint activity in the high-risk group, which also exhibited heightened sensitivity to multiple drugs. In the low-risk group, most genes exhibited a higher mutation rate, and tumor mutational burden (TMB) showed a significant positive correlation with improved prognosis.

1.4. Conclusion

Our study established a signature of mitophagy-related lncRNAs, offering potential for clinical prediction and aiding in the advancement of personalized treatment approaches for STAD patients.

2. Introduction

Gastric cancer exhibits significant molecular and phenotypic diversity, ranking fifth in global incidence and fourth in mortality, notably prevalent in East Asia, Eastern Europe, and South America [1]. Treatment strategies for gastric cancer have seen substantial advancements in recent years. Despite the availability of surgery, chemotherapy, radiotherapy, molecular targeted therapy, immunotherapy, and combined approaches for advanced stages, prognosis remains par-

ticularly grim, especially in later stages of the disease [2, 3]. Delayed diagnosis at advanced stages underscores the urgent necessity for identifying novel and effective tumor markers to enhance diagnostic accuracy and prognosis evaluation in gastric cancer [1]. Mitophagy, a subset of autophagy, involves the removal of damaged or dysfunctional mitochondria through sequestration into autophagosomes for degradation. This process plays a crucial role in maintaining mitochondrial quality and quantity [4]. Increasing evidence from recent studies indicates that dysregulated mitophagy significantly contributes to the onset and progression of cancer [5]. Previous research in gastric cancer has linked activation of the mitophagy pathway to tumor persistence and metastasis [6]. Specifically, studies have shown that inhibiting mitophagy could potentially overcome docetaxel resistance in gastric cancer patients [6]. Additionally, inhibition of mitophagy has been demonstrated to enhance susceptibility of gastric cancer cells to TNF-induced apoptosis in separate investigations [7]. Long non-coding RNAs (lncRNAs) are a class of non-coding RNAs pivotal in regulating chromatin dynamics, gene expression, growth, differentiation, and development [8]. They exhibit dual roles in cancer biology, acting either as tumor suppressors or promoters of malignancy. Notably, their tumor-specific expression patterns and stability in bodily fluids such as plasma and urine offer promising avenues for cancer detection and therapeutic development. Furthermore, the expression levels of lncRNAs hold potential as prognostic indicators for cancer patients [9]. Although it has been established that mitophagy is significantly correlated with tumor progression and chemotherapy efficacy in gastric cancer, the function of mitophagy-associated lncRNAs in STAD remains poorly understood. Consequently, our study endeavors to employ bioinformatics approaches to establish a prognostic risk signature using mitophagy-related lncRNAs. We seek to investigate how this signature correlates with the prognosis and tumor microenvironment of STAD patients, aiming to enhance prognostic predictions and offer insights into personalized treatment strategies.

3. Material and Methods

3.1. Data Gathering and Processing

We collected RNA-Seq data from The Cancer Genome Atlas (TCGA) database, comprising 375 STAD tissues and 32 normal lung tissues. After excluding patients with incomplete survival data and aligning expression profiles with clinical records, we randomly allocated 371 STAD patients into a training set (n = 186) and a testing set (n = 185) using the "caret" package. There were no significant differences in clinical characteristics between these two groups (detail information in Table 1). The training set was utilized for developing the model, and both the testing and full datasets were employed for validating the model.

Table 1: Clinical Information.

Covariates	Type	Training set	Testing set	Entire set	Pvalue
		（N=186）	(N=185)	(N=371)	
Age	<=65	117(46.06%)	122(48.22%)	239(47.14%)	0.5653
	>65	134(52.76%)	124(49.01%)	258(50.89%)	
	unknow	3(1.18%)	7(2.77%)	10(1.97%)	
Gender	FEMALE	135(53.15%)	137(54.15%)	272(53.65%)	0.8912
	MALE	119(46.85%)	116(45.85%)	235(46.35%)	
Stage	Stage I	138(54.33%)	134(52.96%)	272(53.65%)	0.2391
	Stage II	63(24.8%)	57(22.53%)	120(23.67%)	
	Stage III	41(16.14%)	40(15.81%)	81(15.98%)	
	Stage IV	8(3.15%)	18(7.11%)	26(5.13%)	
	unknow	4(1.57%)	4(1.58%)	8(1.58%)	
T	T1	92(36.22%)	77(30.43%)	169(33.33%)	0.6038
	T2	131(51.57%)	140(55.34%)	271(53.45%)	
	T3	21(8.27%)	24(9.49%)	45(8.88%)	
	T4	10(3.94%)	9(3.56%)	19(3.75%)	
	unknow	0(0%)	3(1.19%)	3(0.59%)	
M	M0	178(70.08%)	160(63.24%)	338(66.67%)	0.0739
	M1	8(3.15%)	17(6.72%)	25(4.93%)	
	unknow	68(26.77%)	76(30.04%)	144(28.4%)	
N	N0	164(64.57%)	163(64.43%)	327(64.5%)	0.5532
	N1	49(19.29%)	46(18.18%)	95(18.74%)	
	N2	36(14.17%)	35(13.83%)	71(14%)	
	N3	0(0%)	2(0.79%)	2(0.39%)	
	unknow	5(1.97%)	7(2.77%)	12(2.37%)	

3.2. Identification of Mitophagy Related Genes and Mitophagy Related Lncrnas

We extracted 94 mitophagy-related genes (MRGs) from two previously published articles (refer to Supplementary Table 1) [10, 11]. Subsequently, using the "R" software and the "gencode.v23.annotation.tif" file, we screened the STAD expression profile for lncRNAs and mRNAs. Co-expression analysis (Pearson correlation coefficient ≥ 0.4, $p < 0.001$) was use to identified mitophagy-related lncRNAs (MRlncRNAs), meanwhile differentially expressed lncRNAs (DElncRNAs) was also selected employing the "limma" R package with filter criteria: $|\log2FC| > 1$, FDR < 0.05, and P < 0.05). Finally, we selected shared lncRNAs from MRlncRNAs and DElncRNAs for following analyses.

Supplementary Table 1: 94 mitophagy related genes.

Genes	Description
ABCE1	ATP Binding Cassette Subfamily E Member 1
AMBRA1	Autophagy And Beclin 1 Regulator 1
ATG12	Autophagy Related 12
ATG13	Autophagy Related 13
ATG14	Autophagy Related 14
ATG5	Autophagy Related 5
ATG7	Autophagy Related 7
ATG9A	Autophagy Related 9A
BCL2L1	BCL2 Like 1
BCL2L13	BCL2 Like 13
BECN1	Beclin 1
BNIP3	BCL2 Interacting Protein 3
BNIP3L	BCL2 Interacting Protein 3 Like
CALCOCO2	Calcium Binding And Coiled-Coil Domain 2
CISD1	CDGSH Iron Sulfur Domain 1
CLEC16A	C-Type Lectin Domain Containing 16A
CNOT4	CCR4-NOT Transcription Complex Subunit 4
CSNK2A1	Casein Kinase 2 Alpha 1
CSNK2A2	Casein Kinase 2 Alpha 2
CSNK2B	Casein Kinase 2 Beta
DNM1L	Dynamin 1 Like
E2F1	E2F Transcription Factor 1
FANCC	FA Complementation Group C
FBXO7	F-Box Protein 7
FIS1	Fission, Mitochondrial 1
FKBP8	FKBP Prolyl Isomerase 8
FOXO3	Forkhead Box O3
FUNDC1	FUN14 Domain Containing 1
GABARAP	GABA Type A Receptor-Associated Protein
GABARAPL1	GABA Type A Receptor Associated Protein Like 1
GABARAPL2	GABA Type A Receptor Associated Protein Like 2
HDAC6	Histone Deacetylase 6
HIF1A	Hypoxia Inducible Factor 1 Subunit Alpha
HRAS	HRas Proto-Oncogene, GTPase
HTRA2	HtrA Serine Peptidase 2
HUWE1	HECT, UBA And WWE Domain Containing E3 Ubiquitin Protein Ligase 1
KRAS	KRAS Proto-Oncogene, GTPase
MAP1LC3A	Microtubule Associated Protein 1 Light Chain 3 Alpha
MAP1LC3B	Microtubule Associated Protein 1 Light Chain 3 Beta

MAP1LC3B2	Microtubule Associated Protein 1 Light Chain 3 Beta 2
MAPK10	Mitogen-Activated Protein Kinase 10
MAPK8	Mitogen-Activated Protein Kinase 8
MAPK9	Mitogen-Activated Protein Kinase 9
MFN1	Mitofusin 1
MFN2	Mitofusin 2
MTERF3	Mitochondrial Transcription Termination Factor 3
MTX1	Metaxin 1
MUL1	Mitochondrial E3 Ubiquitin Protein Ligase 1
NBR1	NBR1 Autophagy Cargo Receptor
OPA1	OPA1 Mitochondrial Dynamin Like GTPase
OPTN	Optineurin
PELO	Pelota MRNA Surveillance And Ribosome Rescue Factor
PGAM5	PGAM Family Member 5, Mitochondrial Serine/Threonine Protein Phosphatase
PHB	Prohibitin
PHB2	Prohibitin 2
PINK1	PTEN Induced Kinase 1
PRKAA1	Protein Kinase AMP-Activated Catalytic Subunit Alpha 1
PRKN	Parkin RBR E3 Ubiquitin Protein Ligase
RAB7A	RAB7A, Member RAS Oncogene Family
RHOT1	Ras Homolog Family Member T1
RNF41	Ring Finger Protein 41
RPS27A	Ribosomal Protein S27a
SNCA	Synuclein Alpha
SPATA18	Spermatogenesis Associated 18
SQSTM1	Sequestosome 1
SRC	SRC Proto-Oncogene, Non-Receptor Tyrosine Kinase
TAX1BP1	Tax1 Binding Protein 1
TBC1D15	TBC1 Domain Family Member 15
TBC1D17	TBC1 Domain Family Member 17
TBK1	TANK Binding Kinase 1
TFE3	Transcription Factor Binding To IGHM Enhancer 3
TFEB	Transcription Factor EB
TIGAR	TP53 Induced Glycolysis Regulatory Phosphatase
TOMM20	Translocase Of Outer Mitochondrial Membrane 20
TOMM22	Translocase Of Outer Mitochondrial Membrane 22
TOMM40	Translocase Of Outer Mitochondrial Membrane 40
TOMM5	Translocase Of Outer Mitochondrial Membrane 5
TOMM6	Translocase Of Outer Mitochondrial Membrane 6
TOMM7	Translocase Of Outer Mitochondrial Membrane 7
TOMM70	Translocase Of Outer Mitochondrial Membrane 70
TP53	Tumor Protein P53
UBA52	Ubiquitin A-52 Residue Ribosomal Protein Fusion Product 1
UBB	Ubiquitin B
UBC	Ubiquitin C
UBE2L3	Ubiquitin Conjugating Enzyme E2 L3
ULK1	Unc-51 Like Autophagy Activating Kinase 1
USP15	Ubiquitin Specific Peptidase 15

USP30	Ubiquitin Specific Peptidase 30
USP8	Ubiquitin Specific Peptidase 8
VCP	Valosin Containing Protein
VDAC1	Voltage Dependent Anion Channel 1
VDAC2	Voltage Dependent Anion Channel 2
VPS13C	Vacuolar Protein Sorting 13 Homolog C
VPS13D	Vacuolar Protein Sorting 13 Homolog D

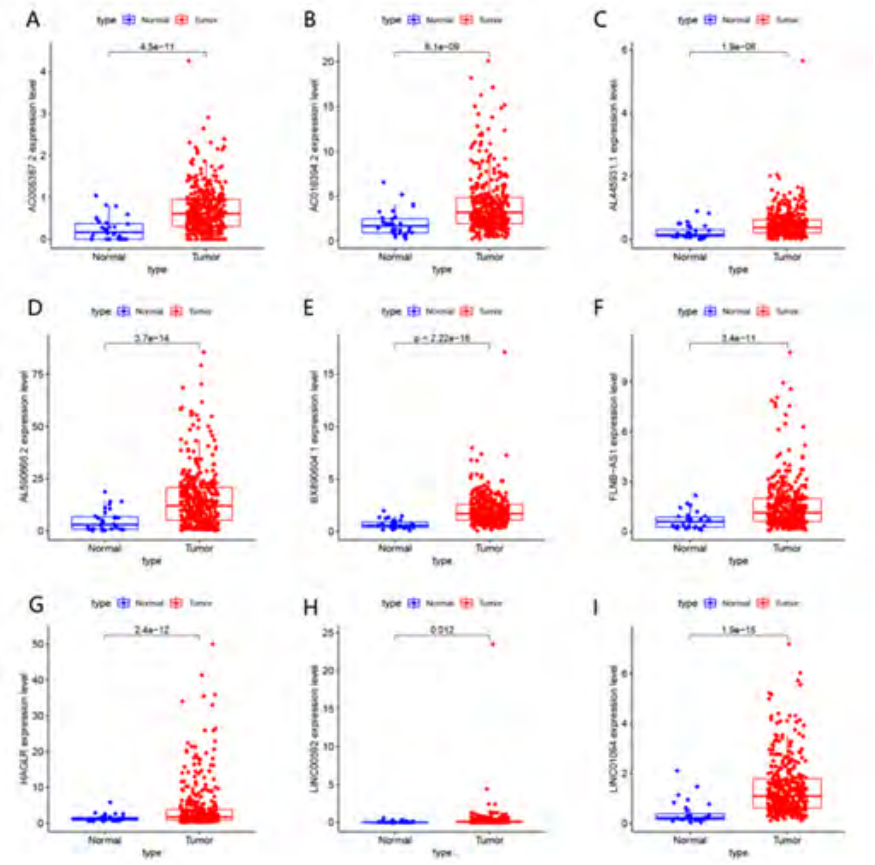

Supplementary Figure 1: Expression of 9 MRlncRNAs in TCGA-STAD cohort.

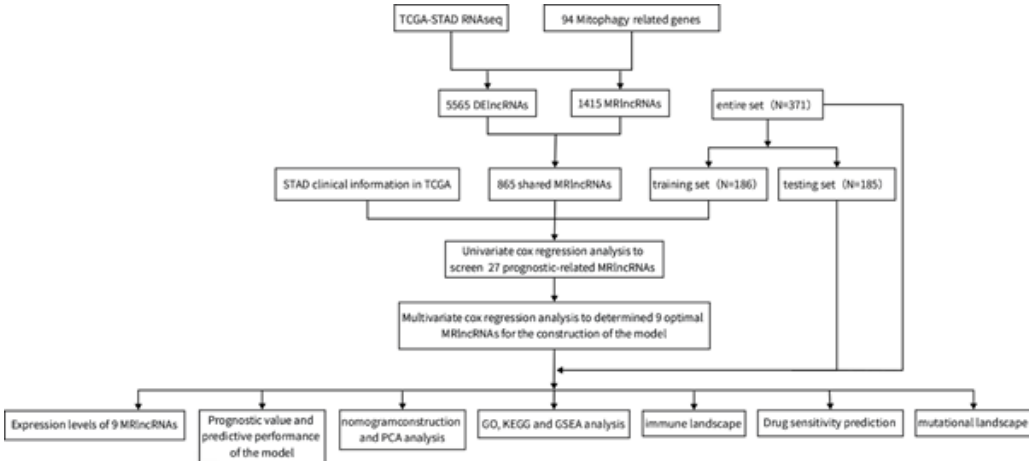

Figure 1: The research flow chart was shown in.

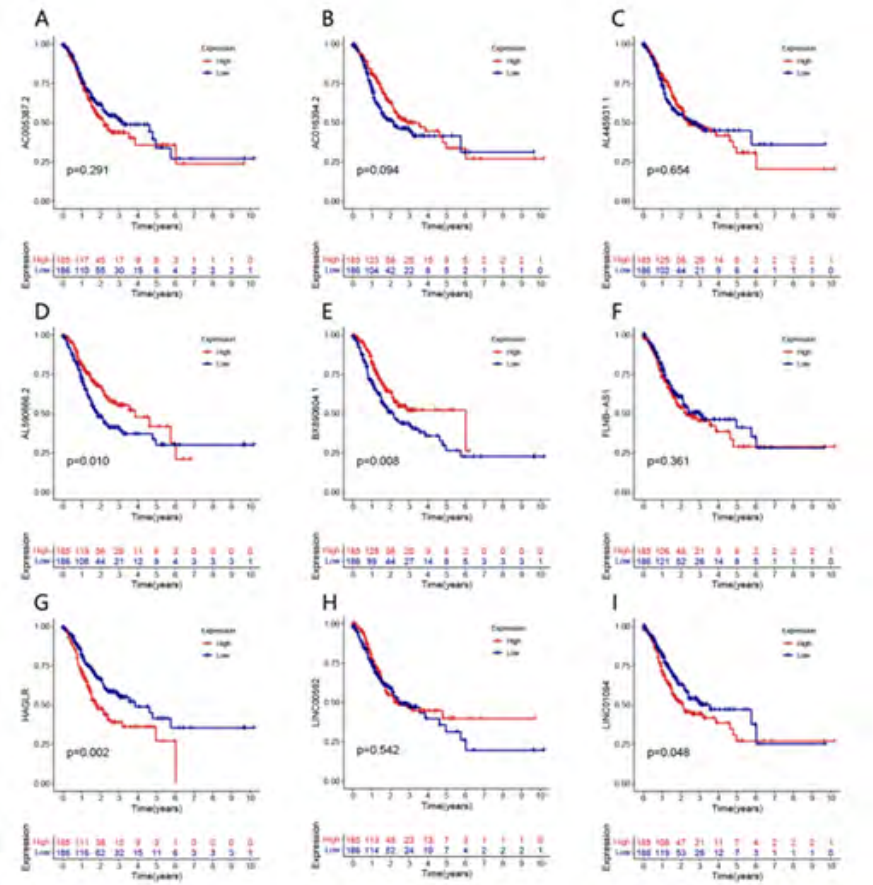

Supplementary Figure 2. Effects of high- and low-expression of the 9 MRlncRNAs on OS in STAD patients.

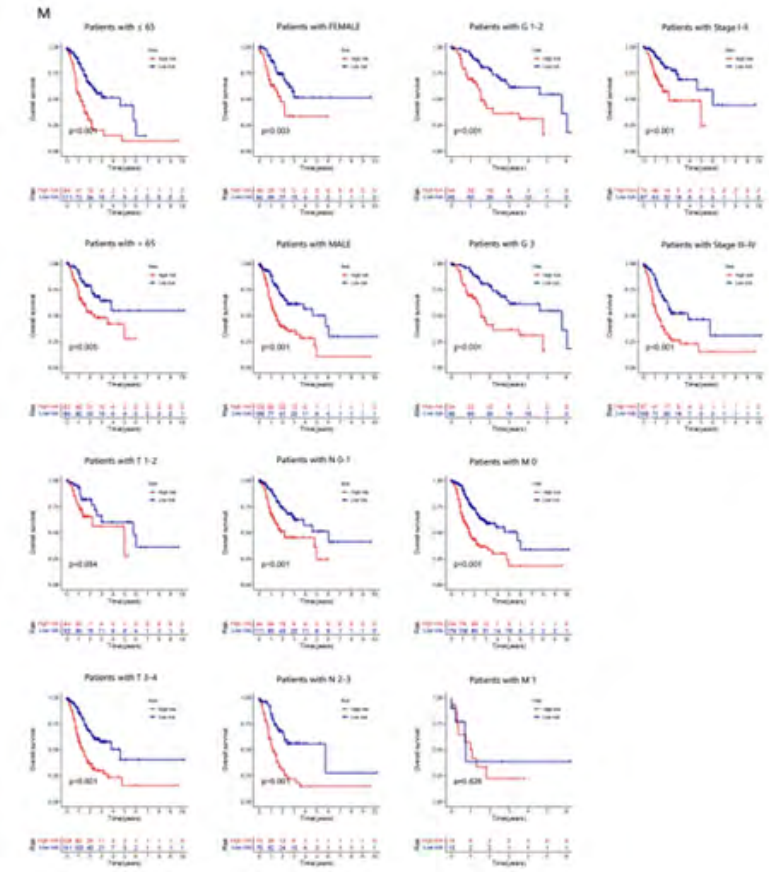

Supplementary Figure 3. Relationship between common clinicopathological features and risk scores.

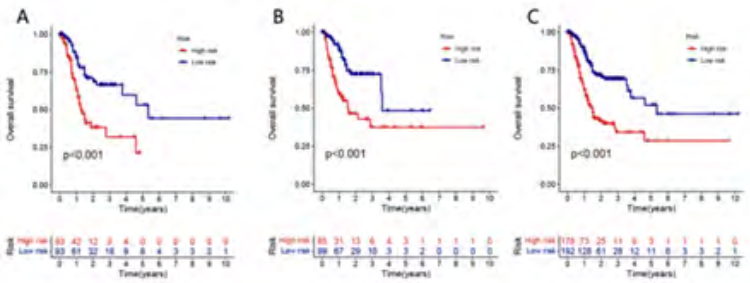

Supplementary Figure 4. K-M curves of progression-free survival (PFS) in (A) training set, (B) testing set and (C) entire set.

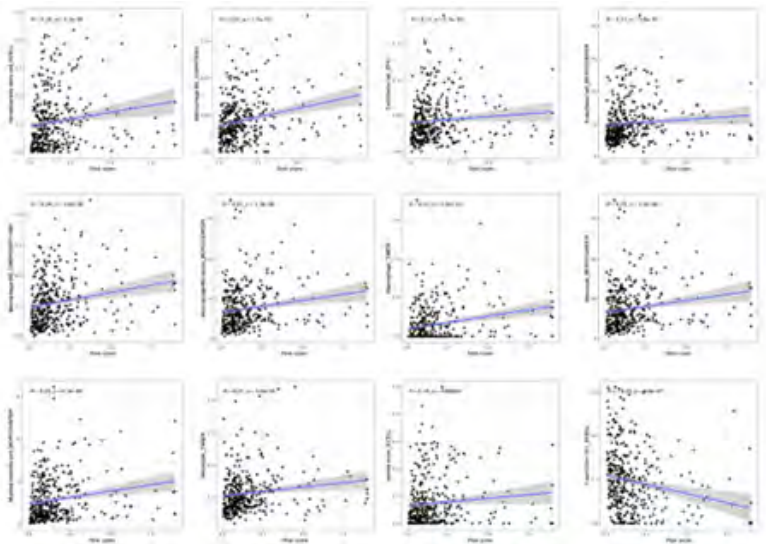

Supplementary Figure 5. Presentation of immune cells with higher correlation coefficients with risk scores in seven platforms.

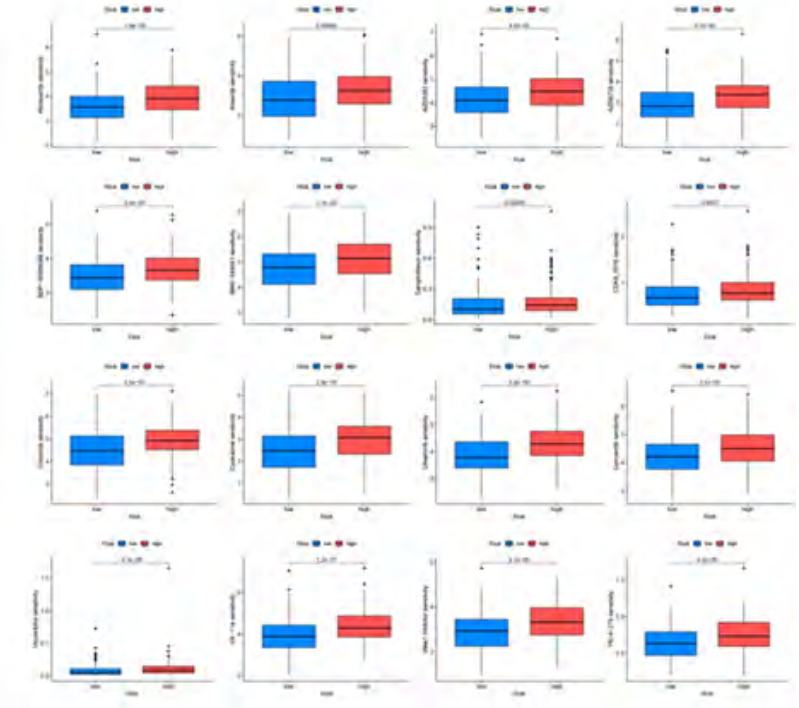

Supplementary Figure 6. Partial presentation of the remaining sensitive drugs in the high-risk group.

3.3. Construction of the Risk Signature

We initially identified prognostic MRlncRNAs through univariate Cox regression analysis. Subsequently, we employed the Least Absolute Shrinkage and Selection Operator (LASSO) regression to mitigate overfitting. Finally, utilizing multivariate Cox regression analysis, we pinpointed the most influential candidate lncRNAs to construct a risk signature. The risk score was computed using the formula provided below:

$$\text{Risk Scores}=\sum \text{Coef}\ (i)^{*}\text{Exp}(i)$$

N represents the number of MRlncRNAs in the risk prognosis signature, Exp(i) represents the expression value of each lncRNA, and Coef(i) represents the regression coefficient of each lncRNA in the multivariate Cox regression analysis.

3.4. Evaluation of the Predictive Performance of the Risk Signature

The risk score for each STAD patient was calculated using the multivariate Cox regression formula, with the median score used to stratify patients into high-risk and low-risk groups. To assess the prognostic value of this risk signature, we analyzed overall survival (OS) and generated survival status plots, along with a heatmap displaying the expression levels of signature lncRNAs based on the risk scores. Uni- and multi- Cox regression analyses were conducted to evaluate the risk signature, respectively. Furthermore, time-dependent receiver operating characteristic (ROC) curves and the concordance index (C-index) were employed to gauge the prognostic accuracy of the risk signature. These analyses utilized the "pheatmap", "survival", "survminer", and "timeROC" packages.

3.5. Nomogram and Calibration

To predict and evaluate the survival rates of STAD patients at 1, 3, and 5 years, we constructed a nomogram integrating the risk score with clinicopathological characteristics. Additionally, calibration curves were generated to assess the consistency between predicted and observed survival rates.

3.6. Principal Component Analysis and Function Enrichment Analysis

Principal component analysis (PCA) was employed to examine the distribution of samples with high and low risk scores using the "limma" and "scatterplot3d" packages. Differential expression analysis was conducted to identify genes (DEGs) with |Log2FC| > 1 and p < 0.05 between the low- and high-risk groups. Gene ontology (GO) analysis encompassed three domains: biological process (BP), cellular component (CC), and molecular function (MF). Additionally, Kyoto Encyclopedia of Genes and Genomes (KEGG) pathway analysis was performed. Furthermore, Gene Set Enrichment Analysis (GSEA) was employed to elucidate pathway enrichment differences between the high- and low-risk groups. These function enrichment analyses utilized tools such as the "cluster Profiler", "org. Hs.eg.db", "enrichplot", "circlize", "RColorBrewer", and "Complex Heatmap" packages.

3.7. Investigation of Tumor Microenvironment

Initially, we utilized the ESTIMATE algorithm to assess the abundance of immune cells and stromal cells across various groups, calculating stromal scores, immune scores, and overall ESTIMATE scores for each group. Subsequently, we characterized the immune infiltration landscape of the TCGA-STAD dataset using seven algorithms (XCELL, TIMER, QUANTISEQ, MCPCOUNTER, EPIC, Cibersort-ABS, and CIBERSORT) and analyzed differences in immune cell content among different risk groups using the Wilcoxon signed rank test, as well as the "limma", "scales", "ggtext", "reshape2", and "tidyverse" packages. We then investigated variations in immune checkpoint expression between high- and low-risk groups, illustrating findings with box plots. Finally, we assessed the risk of immune evasion following immunotherapy for each risk group.

3.8. Drug Senstivity and Tumor Mutation Burden

The "Drug Predictions" file was used to assess drug sensitivity in patients of two groups, which can be used to guide clinical medication in STAD patients. Then, tumor mutation burden (TMB) was calculated using the "maftools" package, and all STAD patients were divided into two groups (high TMB and low TMB) based on a median TMB score. Pearson correlation analysis was also used to determine how well the risk signature and TMB worked together.

4. Result

4.1. Construction of Mitophagy Related lncRNA Risk Predictive Signature

The research flow chart was shown in Figure 1. A total of 1415 MRlncRNAs were identified utilizing co-expression analysis between 94 MRGs and lncRNAs in STAD cohort. Next, 5565 DElncRNAs were obtained by differential expression analysis between normal tissues and STAD tissues (Figure 2A). Subsequently, 865 shared lncRNAs of MRlncRNAs and DElncRNAs were gained (Figure 2B). 27 prognostic related MRlncRNAs were screened in training sets using univariate Cox analysis ($p< 0.05$) (Figure 2C). Next, LASSO regression analysis was then used to identify the 13 MRlncRNAs, avoiding overfitting. (Figure 2D, E) Finally, we used multivariate Cox regression analysis to generate 9 MRlncRNAs (AC005387.2, LINC01094, AL590666.2, LINC00592, BX890604.1, AL445931.1, HAGLR, AC016394.2, FLNB−AS1), which were best suited to building risk signature.

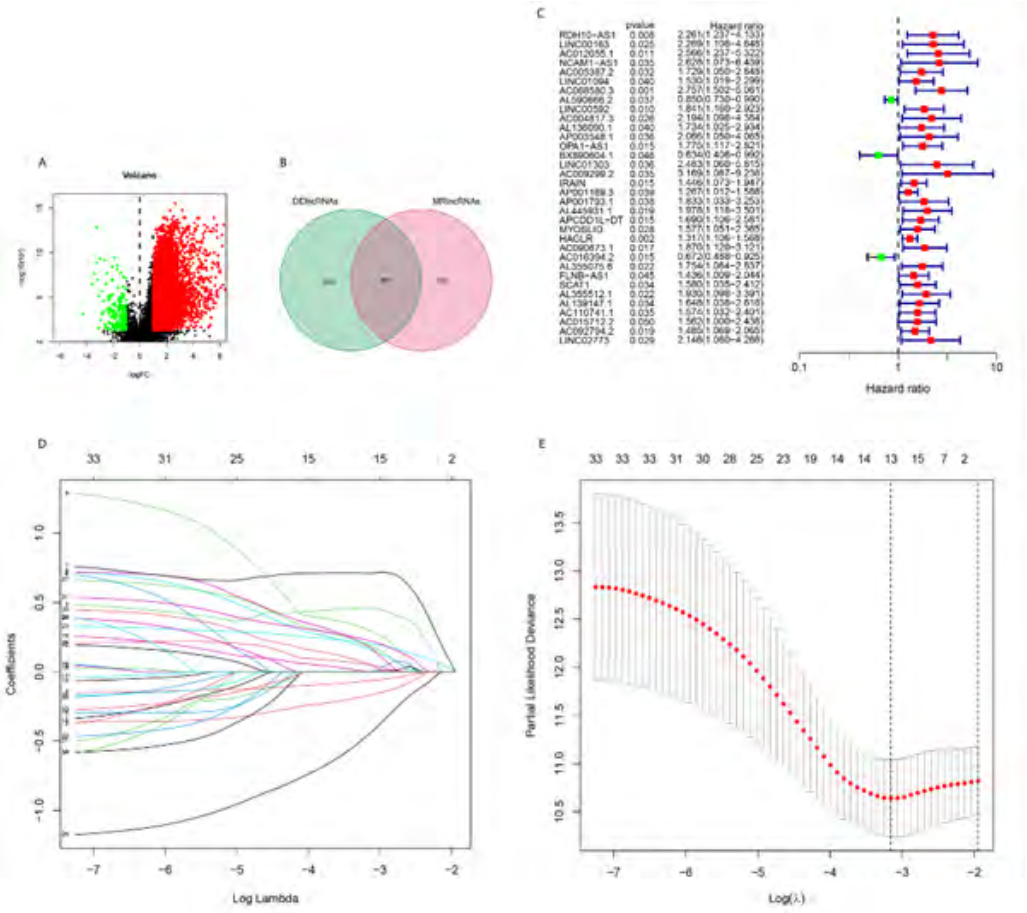

Figure 2a, b, c and d: A total of 1415 MRlncRNAs were identified utilizing co-expression analysis between 94 MRGs and lncRNAs in STAD cohort. Next, 5565 DElncRNAs were obtained by differential expression analysis between normal tissues and STAD tissues (Figure 2A). Subsequently, 865 shared lncRNAs of MRlncRNAs and DElncRNAs were gained (Figure 2B). 27 prognostic related MRlncRNAs were screened in training sets using univariate Cox analysis ($p < 0.05$) (Figure 2C). Next, LASSO regression analysis was then used to identify the 13 MRlncRNAs, avoiding overfitting. (Figure 2D, E)

4.2. Survival Prediction Value of The Signature

The patients were divided into high- and low-risk groups based on the median risk score cutoff value. By analyzing the risk score distribution, survival status, survival time, and the KM curves of overall survival in the entire set, the training set, and the testing set, separately, all patients in the high-risk cohort had significantly worse prognoses (Figure 3). Applying the area under the ROC curve (AUC), we evaluated the prognostic sensitivity and specificity of the risk signature. The 1-, 3-, and 5-year AUCs of the training set were 0.804, 0.764, and 0.874, of the testing set were 0.664, 0.600, and 0.635 and of entire set were 0.726, 0.681, and 0.735, respectively (Figure 4G-I). In addition, the risk score had a higher AUC (AUC =0.740) than other clinicopathology characteristics (Age, AUC=0.594, Gender, AUC=0.522, Grade, AUC=0.561, Stage, AUC=0.602) (Figure 4J). C-index was higher than 60% within 5 years and better than other clinicopathological factors. These results suggest that the risk signature has promising predictive capabilities (Figure 4K).

4.3. An Independent Prognostic Indicator of STAD of the Mitophagy Related Lncrna Signature

In the training set, univariate independent prognostic analysis revealed that the risk score ($p < 0.001$, HR = 1.153) and tumor stage ($p = 0.002$, HR = 1.537), both of which were high-risk factors, can be used as independent prognostic factors (Figure 4A). In addition, multivariate independent prognostic analysis revealed that risk score ($p < 0.001$, HR = 1.150), tumor stage ($p < 0.001$, HR = 1.675) can be used as high-risk independent prognostic factors (Figure 4D). Independent univariate and multivariate prognostic analyses of the entire and testing sets produced results that were consistent with the training set (Figure 4B, C, E, F).

4.4. Construction and Validation of Nomogram

To assess the validity and accuracy of risk signature, we constructed nomogram to predict 1-, 3-, and 5-year survival in patients with STAD (Figure 5A). The calibration curve demonstrated a high degree of concordance between actual and predicted nomogram results (Figure 5B).

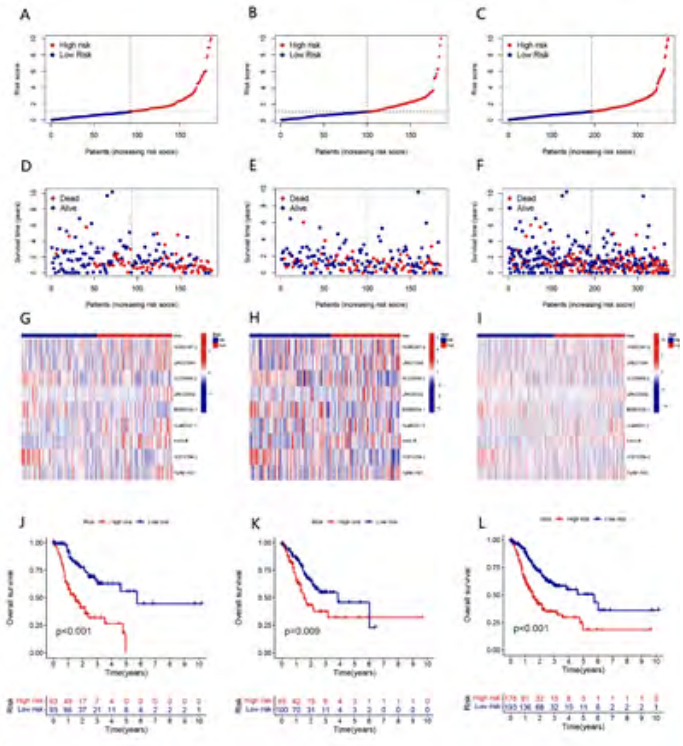

Figure 3: The patients were divided into high- and low-risk groups based on the median risk score cutoff value. By analyzing the risk score distribution, survival status, survival time, and the KM curves of overall survival in the entire set, the training set, and the testing set, separately, all patients in the high-risk cohort had significantly worse prognoses.

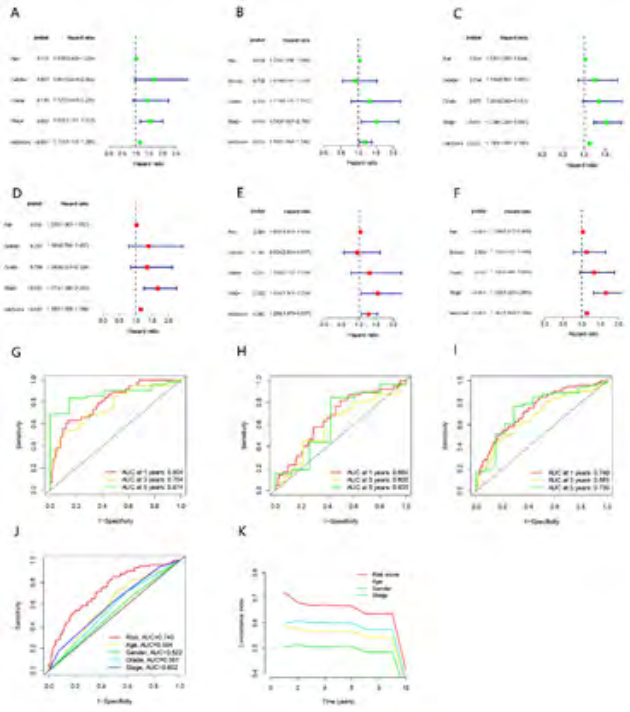

Figure 4: Applying the area under the ROC curve (AUC), we evaluated the prognostic sensitivity and specificity of the risk signature. The 1-, 3-, and 5-year AUCs of the training set were 0.804, 0.764, and 0.874, of the testing set were 0.664, 0.600, and 0.635 and of entire set were 0.726, 0.681, and 0.735, respectively (Figure 4G-I). In addition, the risk score had a higher AUC (AUC =0.740) than other clinicopathology characteristics (Age, AUC=0.594, Gender, AUC=0.522, Grade, AUC=0.561, Stage, AUC=0.602) (Figure 4J). C-index was higher than 60% within 5 years and better than other clinicopathological factors. These results suggest that the risk signature has promising predictive capabilities (Figure 4K).

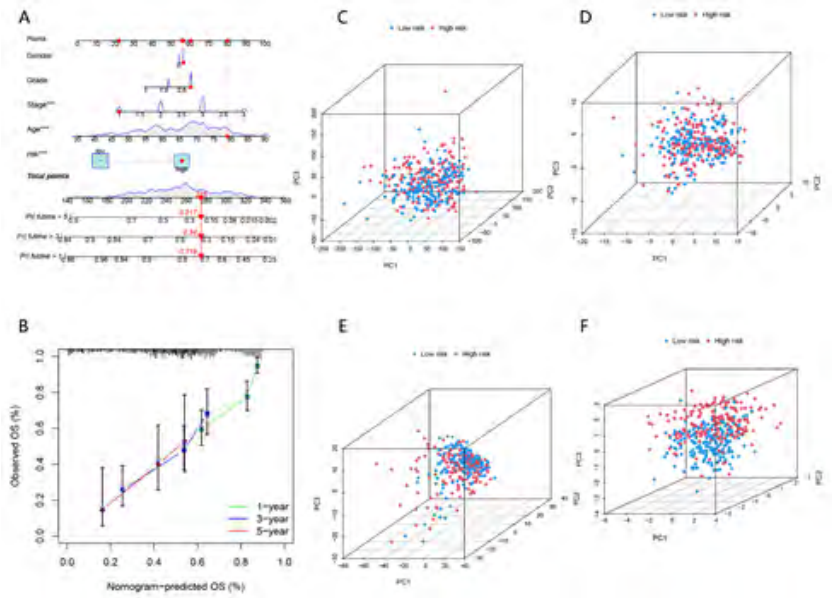

Figure 5: To assess the validity and accuracy of risk signature, we constructed nomogram to predict 1-, 3-, and 5-year survival in patients with STAD.

4.5. The Principal Component Analysis and Biological Pathways Analysis

On the basis of the whole-genome sequencing data of the TCGA-STAD cohort, principal component analysis was performed in all genes, 94 MRGs, 1415 MRlncRNAs, and 9 lncRNAs of risk signature, respectively (Figure 5C-F). According to the 3D scatter plot of PCA, the distribution difference between the two groups based on the risk signature was significant and stable, indicating that the risk signature accurately distinguished STAD patients with a high or low risk, and also reflected the significant difference in the sensitivity of mitophagy between the two groups. We further investigated potential biological mechanisms between high- and low-risk groups, by running GO and KEGG analyses on 197 DEGs between high- and low-risk groups. Signaling receptor activator activity, receptor ligand activity, sulfur compound binding, hormone activity, and peptidase regulator activity were the top five GO terms for biological processes. The top five GO terms for cellular components were collagen-containing extracellular matrix, endoplasmic reticulum lumen, blood microparticle, protein-lipid complex, and lipoprotein particle. Regulation of lipid metabolic process, digestion, positive regulation of hormone secretion, regulation of plasma lipoprotein particle levels, and protein-lipid complex subunit organization, were among the top five GO terms for molecular functions (Figure 6A). The top five KEGG signaling pathways were Neuroactive ligand-receptor interaction, Fat digestion and absorption, Pancreatic secretion, Protein digestion and absorption, and Vitamin digestion and absorption (Figure 6B). According to the GSEA analysis, the top five enriched pathways in the high-risk group were complement and coagulation cascades, ECM receptor interaction, glycerolipid metabolism, hematopoietic cell lineage, and neuroactive ligand receptor interaction neuroactive ligand receptor interaction. On the other hand, the top five enriched pathways in the low-risk group were cell cycle, oxidative phoshorylation, ribosome, RNA degaradation, and spliceosome (Figure 6C-D).

4.6. Landscape of Tumor Microenvironment

In terms of TME score, high-risk patients had a higher stromal score, immune score, and estimate score than low-risk patients (Figure 7C-E). On the other hand, we found that a higher risk score was associated with a greater number of immune cells, as demonstrated by the immune cell bubble map. There were more immune cells associated with high-risk groups on various platforms, such as macrophage M1 and Neutrophil on TIMER, Hematopoietic stem cell on XCELL, Macrophage/Monocyte on MCPCOUNTER, Macrophage M2 on QUANTISEQ (all $p<0.05$) (Figure 7A). The differences of the expression of immune checkpoints between the two groups were then investigated further. The majority of immune checkpoints were found to be more activated in the high-risk group (Figure 7F). Subsequently, the sensitivity of immunotherapy in high- and low-risk group was further investigated by using TIDE algorithm. The result showed that the TIDE level in the low-risk group was lower than that in the high-risk group, indicating that the patients in the low-risk group were less likely to suffer from immune escape and were more likely to benefit from immunotherapy (Figure 7B).

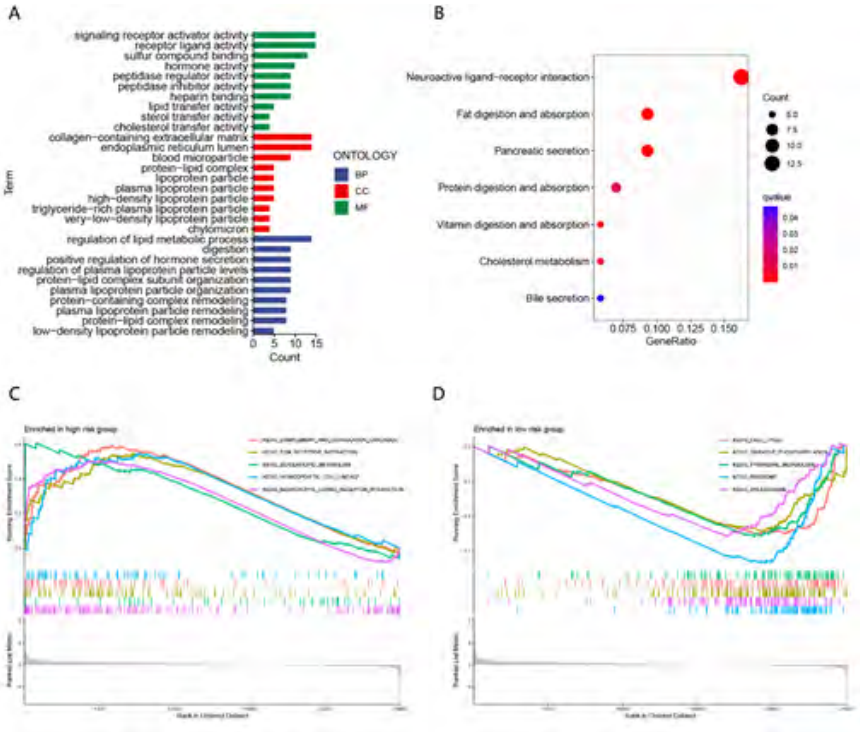

Figure 6: The top five GO terms for cellular components were collagen-containing extracellular matrix, endoplasmic reticulum lumen, blood microparticle, protein-lipid complex, and lipoprotein particle. Regulation of lipid metabolic process, digestion, positive regulation of hormone secretion, regulation of plasma lipoprotein particle levels, and protein-lipid complex subunit organization, were among the top five GO terms for molecular functions.

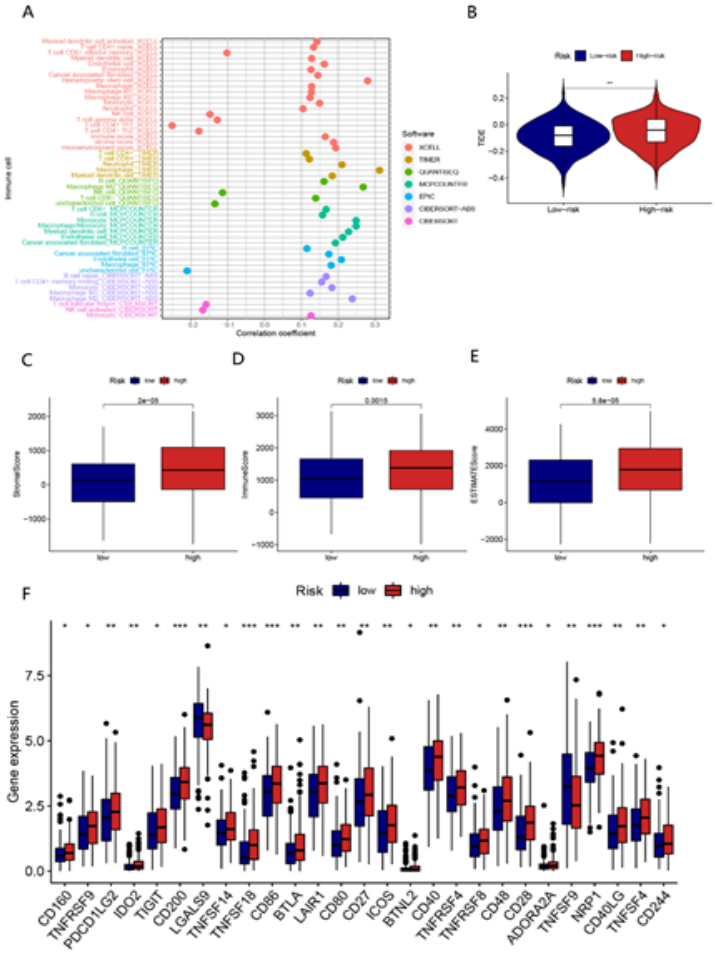

Figure 7: In terms of TME score, high-risk patients had a higher stromal score, immune score, and estimate score than low-risk patients.

4.7. Drug Susceptibility and TMB Analysis

In STAD patients, we analyzed the drug sensitivity of 198 drugs included in the "Drug Predictions" file to identify and demonstrate the medications used to effectively treat STAD patients. The high-risk group was more sensitive to most drugs, including 5-Fluorouracil, Acetalax, Afatinib, and so on. While the low-risk group was more sensitive to BMS-754807, Doramapimod, and JQ1(Figure 8F). We used maftools algorithm to study the mutation of high- and low-risk groups, and the results showed that there was a significant difference in TMB between the high and low risk groups ($p< 0.001$). For most genes, the mutation rate of low- risk group was higher than that of high-risk group, but P53 mutation rate in high-risk group was higher than that in low-risk group. In addition. We further analyzed the effect of TMB on OS and found that patients with high TMB had better OS than those with low TMB (Figure 8A-E).

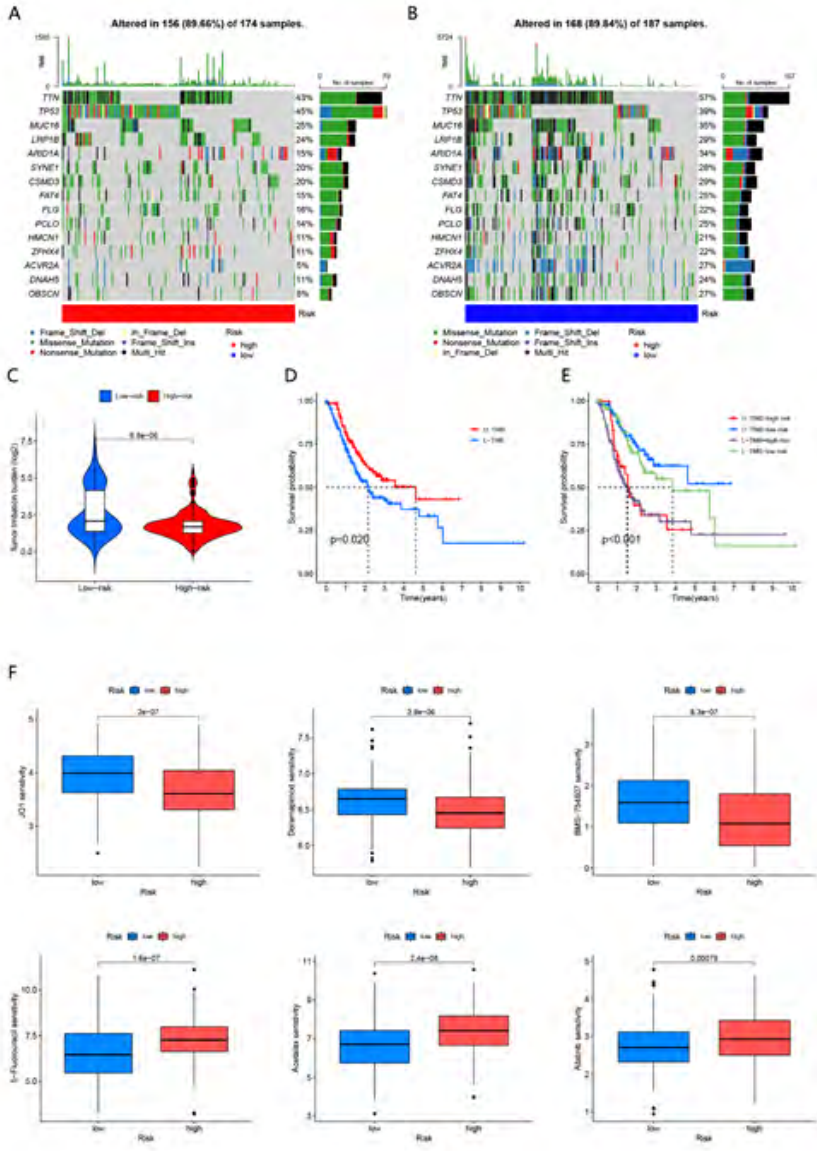

Figure 8: In STAD patients, we analyzed the drug sensitivity of 198 drugs included in the "Drug Predictions" file to identify and demonstrate the medications used to effectively treat STAD patients. The high-risk group was more sensitive to most drugs, including 5-Fluorouracil, Acetalax, Afatinib, and so on. While the low-risk group was more sensitive to BMS-754807, Doramapimod, and JQ1.

5. Discussion

STAD ranks among the most prevalent malignancies globally, and despite significant therapeutic advances in recent years, its prognosis remains bleak. Therefore, urgent efforts are required to identify meaningful molecular biomarkers that can improve prognosis prediction and evaluation in STAD patients. Mitophagy, a pivotal mechanism in cellular mitochondrial quality control, exhibits dual roles in malignancies, contingent upon tumor type, growth stage, and the presence of cancer stem cells [12]. Despite notable progress in understanding the interplay between cancer and mitophagy, research on mitophagy-related cancer markers remains limited. Long non-coding RNAs (lncRNAs) play a critical role in tumor progression, with numerous studies highlighting their potential as molecular biomarkers [9, 13]. For instance, Nan et al. identified circulating lncRNA XLOC

009167 as a diagnostic biomarker for lung cancer [14]. In this study, we identified mitophagy-related lncRNA markers that hold promise for predicting the prognosis of STAD patients. This study identified 9 mitophagy-related lncRNAs (AC005387.2, LINC01094, AL590666.2, LINC00592, BX890604.1, AL445931.1, HAGLR, AC016394.2, FLNB-AS1) through LASSO regression, as well as univariate and multivariate Cox regression analyses. These lncRNAs show promise as biomarkers for stratifying diagnosis and predicting prognosis in patients with STAD. Based on their median risk scores, patients were categorized into high- and low-risk groups. Kaplan-Meier curves illustrated significantly poorer prognoses among high-risk patients compared to their low-risk counterparts. The prognostic signature comprises 9 mitophagy-related lncRNAs. LINC01094 has been implicated in driving the progression of various cancers. Jing et al. demonstrated its role in enhancing proliferation, migration, invasion, and EMT in OC cells by sequestering miR-57715 [15]. Recent research indicates that heightened expression of LINC01094 correlates with a poorer prognosis in gastric cancer, linked to the epithelial-mesenchymal transition pathway and macrophage infiltration [16]. Can et al. identified LINC00592 as a prognostic marker in gastric cancer [17]. Moreover, LINC00592 has been utilized as a ferroptosis-related lncRNA in constructing a risk signature for lung cancer [18]. Suggesting potential connections between mitophagy and ferroptosis. Jing et al. also linked HAGLR to chemotherapy resistance in gastric cancer [19], and used it as an autophagy-related lncRNA to formulate a prognostic model for gastric cancer [20]. Furthermore, several studies have highlighted HAGLR's role in promoting hepatocellular carcinoma, breast cancer, and colon cancer development [21-23]. The prognostic relevance of the risk signature was investigated in STAD patients. Initially, univariate and multivariate regression analyses confirmed the risk score as an independent predictor of prognosis in STAD patients. Subsequently, an ROC curve was generated, demonstrating the robust predictive capability of this signature, underscoring the significant clinical relevance of MRlncRNAs. Moreover, the risk score outperformed traditional clinicopathological factors such as age and gender in terms of predictive accuracy. Similarly, our C-index curve illustrated superior predictive power of the risk score compared to other clinicopathological indices. To enhance prognostic assessment, a nomogram was developed, showing excellent agreement between predicted and actual outcomes on the calibration curve. Finally, PCA analysis revealed that the 9 lncRNAs comprising the risk signature effectively clustered patients into high- and low-risk groups. We further performed functional analysis of DEGs between high and low risk groups to explore possible pathways and functions of the signature. GO and KEGG analysis showed that DEGs were mainly concentrated in the molecular biological functions and pathways related to digestive absorption, suggesting that 9 MRlncRNAs may be involved in the development of tumors by regulating energy metabolism. GSEA analysis showed that the first five enrichment pathways in the high-risk group were complement and coagulation cascades, ECM receptor interaction, glycerolipid metabolism, hematopoietic cell lineage, and neuroactive ligand receptor interaction neuroactive ligand receptor interaction. Extracellular matrix (ECM) is one of the most important regulators of cell and tissue function in the body [24]. The extracellular matrix is intricately involved in the development and advancement of gastric cancer [25]. According to Ling et al., the analysis of pivotal genes in gastric cancer identified ECM receptor interaction and adhesion as significant mechanisms in GC [26]. Additionally, Min et al. demonstrated that ELK3 regulates the migration and invasion of gastric cancer cells by modulating genes associated with ECM remodeling [27]. The tumor microenvironment (TME) comprises diverse immune cells, stromal cells, and extracellular components that significantly influence tumorigenesis, progression, and resistance to treatment [28]. Immune cells are pivotal within the TME, correlating with various levels of tumor progression and patient survival [29]. Consequently, we conducted a deeper investigation into immune cell infiltration within tumor tissues. TME analysis revealed significantly higher immune scores, stromal scores, and estimate scores in high-risk groups. Subsequently, we applied seven common algorithms to assess the immune infiltration status of STAD patients. Our findings indicated that patients with high-risk scores exhibited markedly lower levels of CD4+ T cells and significantly higher levels of M2 macrophages. CD4+ T cells play a critical role in enhancing CTL-mediated antitumor responses, employing multiple mechanisms to eliminate tumor cells and potentially improving outcomes of immunotherapy [30]. In contrast, M2 macrophages exhibit reduced antigen-presenting capabilities compared to M1 macrophages31. They secrete factors that suppress T cell proliferation and activity, thereby promoting angiogenesis and tissue repair [31]. Emerging evidence highlights that tumor-associated macrophages (TAMs) often exhibit a polarized M2 phenotype. Yu et al. confirmed that tumors facilitate metastasis in gastric and breast cancers by recruiting M2 macrophages that secrete CHI3L [31]. Increasing evidence demonstrates that tumor-associated macrophages (TAM) are polarized M2 macrophages. Yu et al. [32]. Confirmed that tumors promote gastric cancer and breast cancer metastasis by recruiting M2 macrophages, which secrete CHI3L [32]. These findings underscore that patients with high-risk scores may have compromised cancer-fighting abilities and a heightened susceptibility to metastasis. Immune checkpoints regulate the regulatory mechanism of T cell immune responses, while tumor cells exploit these checkpoints to evade immune surveillance [33]. In a pivotal Phase III trial, Nabulizumab significantly extended overall survival in patients with advanced gastric cancer undergoing third-line therapy [34]. Consequently, we evaluated immune checkpoint expression levels in high- and low-risk groups. Most immune checkpoints showed significantly higher expression in the high-risk group, with LGALS9 notably higher in the low-risk group. This suggests not only increased malignancy in high-risk tumors but also enhanced suitability of high-risk patients for immune checkpoint inhibitor

(ICI) therapy. Additionally, TIDE analysis assessed the risk of treatment failure due to immune evasion in STAD patients receiving immunotherapy, revealing markedly higher rates of treatment failure in the high-risk group compared to the low-risk group. Therefore, while the high-risk group may benefit more from ICI treatment, it also presents certain limitations. Comprehensive treatment stands as the cornerstone in managing advanced gastric cancer, demonstrating substantial enhancements in patient prognoses [3]. In STAD patients, our analysis of drug sensitivity among high and low-risk groups revealed compelling findings: the high-risk cohort exhibited heightened sensitivity to a wide array of drugs, such as 5-fluorouracil, Acetaloc, and Afatinib. Conversely, the low-risk group displayed greater responsiveness to BMS-754807, Doramapimod, and JQ1. These insights underscore the preference for tailored drug therapies that favor the high-risk group in clinical practice. Further analysis of TMB revealed that the top 10 mutated genes included PCLO, FLG, FAT4, CSMD3, SYNE1, ARID1A, LRP1B, MUC16, TP53, and TTN. While the low-risk group exhibited a higher overall mutation rate, TP53 and TTN mutations were more prevalent in the high-risk group. Additionally, high TMB correlated positively with improved overall survival (OS) and has been linked to enhanced survival outcomes in various cancers treated with immune checkpoint inhibitors [35]. TP53 is a commonly mutated oncogene in human cancers, with mutation frequency influenced by tumor type, subtype, stage of development, and environmental factors like infections [36] .The geographical distribution of carcinogenic exposures also contributes significantly to TP53 mutation patterns [36]. The impact of TP53 mutations on tumor immunity varies across cancer types; it shows a positive correlation in BRCA and STAD but a negative one in HNSC [37]. TTN ranks as the second most frequently mutated gene in solid tumors and is associated with higher TMB, predicting a favorable response to immune checkpoint blockade [38]. Studies have highlighted TTN mutations as predictors of poor prognosis in thyroid cancer [39]. Consistent with prior research [36-39], our findings indicate that TP53 and TTN are highly correlated with the prognosis of gastric cancer and can be used as immunotherapy targets for gastric cancer. To our knowledge, our study represents the first exploration of the prognostic and immunological implications of a mitophagy-related lncRNA signature in gastric cancer. Nonetheless, it is important to acknowledge certain limitations. Our analysis relies solely on STAD samples from the TCGA database, potentially introducing sample bias and yielding findings that may not be universally applicable. Moreover, the absence of in vivo or in vitro studies limits our ability to fully validate the potential of these lncRNAs as biomarkers and understand their underlying mechanisms.

6. Conclusions

Our study has uncovered a new mitophagy-related lncRNA signature capable of predicting the prognosis of STAD patients and suggesting immunotherapy strategies. We anticipate that this research will deliver positive outcomes for clinical STAD management and advance the field of mitophagy in cancer research.

7. Data availability Statement

The original contributions presented in the study are included in the article/Supplementary Material. Further inquiries can be directed to the corresponding author. The public datasets analyzed in this study can be found in the TCGA (https://portal.gdc.cancer.gov/).

References

1. Smyth EC, Nilsson M, Grabsch HI, van Grieken NC, Lordick F. Gastric cancer. The Lancet. 2020; 396(10251): 635-48.
2. Catalano V, Labianca R, Beretta GD, Gatta G, De Braud F, Van Cutsem E. Gastric cancer. Critical reviews in oncology/hematology. 2009; 71(2): 127-64.
3. Song Z, Wu Y, Yang J, Yang D, Fang X. Progress in the treatment of advanced gastric cancer. Tumor Biology. 2017; 39(7): 1010428317714626.
4. Pickles S, Vigié P, Youle RJ. Mitophagy and quality control mechanisms in mitochondrial maintenance. Current Biology. 2018; 28(4): R170-R85.
5. Panigrahi DP, Praharaj PP, Bhol CS, Mahapatra KK, Patra S, Behera BP. editors. The emerging, multifaceted role of mitophagy in cancer and cancer therapeutics. Seminars in cancer biology. 2020.
6. Yan H, Xiao F, Zou J, Qiu C, Sun W, Gu M. NR4A1-induced increase in the sensitivity of a human gastric cancer line to TNFα-mediated apoptosis is associated with the inhibition of JNK/Parkin-dependent mitophagy. International journal of oncology. 2018; 52(2): 367-78.
7. Kim TW, Lee S-J, Park Y-J, Park SY, Oh BM, Park YS. Opa-interacting protein 5 modulates docetaxel-induced cell death via regulation of mitophagy in gastric cancer. Tumor Biology. 2017; 39(10): 1010428317733985.
8. Bhan A, Mandal SS. LncRNA HOTAIR: A master regulator of chromatin dynamics and cancer. Biochimica et Biophysica Acta (BBA)-Reviews on Cancer. 2015; 1856(1): 151-64.
9. Khandelwal A, Bacolla A, Vasquez KM, Jain A. Long non-coding RNA: A new paradigm for lung cancer. Molecular carcinogenesis. 2015; 54(11): 1235-51.
10. Wang Y, Wang Z, Sun J, Qian Y. Identification of HCC Subtypes with Different Prognosis and Metabolic Patterns Based on Mitophagy. Frontiers in cell and developmental biology. 2021; 9.
11. Chen H, Wang J, Zeng R, Luo Y, Guo K, Wu H. Development and validation of a novel mitophagy-related gene prognostic signature for hepatocellular carcinoma based on immunoscore classification of tumor. Journal of oncology. 2021; 2021.
12. Poole LP, Macleod KF. Mitophagy in tumorigenesis and metastasis. Cellular and Molecular Life Sciences. 2021; 78(8): 3817-51.
13. McCabe EM, Rasmussen TP, editors. lncRNA involvement in cancer stem cell function and epithelial-mesenchymal transitions. Seminars in cancer biology; 2021.
14. Jiang N, Meng X, Mi H, Chi Y, Li S, Jin Z. Circulating lncRNA XLOC_009167 serves as a diagnostic biomarker to predict lung cancer. Clinica Chimica Acta. 2018; 486: 26-33.

15. Xu J, Zhang P, Sun H, Liu Y. LINC01094/miR-577 axis regulates the progression of ovarian cancer. Journal of ovarian research. 2020; 13(1): 1-9.

16. Ye Y, Ge O, Zang C, Yu L, Eucker J, Chen Y. LINC01094 Predicts Poor Prognosis in Patients with Gastric Cancer and is Correlated with EMT and Macrophage Infiltration. Technology in cancer research & treatment. 2022; 21: 15330338221080977.

17. Cheng C, Wang Q, Zhu M, Liu K, Zhang Z. Integrated analysis reveals potential long non-coding RNA biomarkers and their potential biological functions for disease free survival in gastric cancer patients. Cancer Cell International. 2019; 19(1): 1-17.

18. Wang Y, Lu G, Xue X, Xie M, Wang Z, Ma Z. Characterization and validation of a ferroptosis-related LncRNA signature as a novel prognostic model for lung adenocarcinoma in tumor microenvironment. Frontiers in Immunology. 2022; 13.

19. Hu J, Huang L, Ding Q, Lv J, Chen Z. Long noncoding RNA HAGLR sponges miR-338-3p to promote 5-Fu resistance in gastric cancer through targeting the LDHA-glycolysis pathway. Cell Biology International. 2022; 46(2): 173-84.

20. Chen D, Wang M, Xu Y, Jiang X, Xiong L, Zhang L. A novel autophagy-related lncRNA prognostic signature associated with immune microenvironment and survival outcomes of gastric cancer patients. International Journal of General Medicine. 2021; 14: 6935.

21. Sun W, Nie W, Wang Z, Zhang H, Li Y, Fang X. Lnc HAGLR promotes colon cancer progression through sponging miR-185-5p and activating CDK4 and CDK6 in vitro and in vivo. OncoTargets and therapy. 2020; 13: 5913.

22. Li Y, Huang G, Wang W, Zang H. LncRNA HAGLR exacerbates hepatocellular carcinoma through negatively regulating miR-6785-5p. Eur Rev Med Pharmacol Sci. 2020; 24(18): 9353-60.

23. Jin L, Luo C, Wu X, Li M, Wu S, Feng Y. LncRNA-HAGLR motivates triple negative breast cancer progression by regulation of WNT2 via sponging miR-335-3p. Aging (Albany NY). 2021; 13(15): 19306.

24. Cox TR, Erler JT. Remodeling and homeostasis of the extracellular matrix: implications for fibrotic diseases and cancer. Disease models & mechanisms. 2011; 4(2): 165-78.

25. Moreira AM, Pereira J, Melo S, Fernandes MS, Carneiro P. The extracellular matrix: an accomplice in gastric cancer development and progression. Cells. 2020; 9(2): 394.

26. Cao L, Chen Y, Zhang M, Xu D-q, Liu Y, Liu T. Identification of hub genes and potential molecular mechanisms in gastric cancer by integrated bioinformatics analysis. PeerJ. 2018; 6: e5180.

27. Lee M, Cho H-J, Park K-S, Jung H-Y. ELK3 Controls Gastric Cancer Cell Migration and Invasion by Regulating ECM Remodeling-Related Genes. International journal of molecular sciences. 2022; 23(7): 3709.

28. Zeng D, Wu J, Luo H, Li Y, Xiao J, Peng J. Tumor microenvironment evaluation promotes precise checkpoint immunotherapy of advanced gastric cancer. Journal for immunotherapy of cancer. 2021; 9(8).

29. Bremnes RM, Al-Shibli K, Donnem T, Sirera R, Al-Saad S, Andersen S. The role of tumor-infiltrating immune cells and chronic inflammation at the tumor site on cancer development, progression, and prognosis: emphasis on non-small cell lung cancer. Journal of Thoracic Oncology. 2011; 6(4): 824-33.

30. Borst J, Ahrends T, Bąbała N, Melief CJ, Kastenmüller W. CD4+ T cell help in cancer immunology and immunotherapy. Nature Reviews Immunology. 2018; 18(10) :635-47.

31. Qian B-Z, Pollard JW. Macrophage diversity enhances tumor progression and metastasis. Cell. 2010; 141(1): 39-51.

32. Chen Y, Zhang S, Wang Q, Zhang X. Tumor-recruited M2 macrophages promote gastric and breast cancer metastasis via M2 macrophage-secreted CHI3L1 protein. Journal of hematology & oncology. 2017; 10(1): 1-13.

33. Henriksen A, Dyhl-Polk A, Chen I, Nielsen D. Checkpoint inhibitors in pancreatic cancer. Cancer treatment reviews. 2019; 78: 17-30.

34. Kang Y-K, Boku N, Satoh T, Ryu M-H, Chao Y, Kato K. Nivolumab in patients with advanced gastric or gastro-oesophageal junction cancer refractory to, or intolerant of, at least two previous chemotherapy regimens (ONO-4538-12, ATTRACTION-2): a randomised, double-blind, placebo-controlled, phase 3 trial. The Lancet. 2017; 390(10111): 2461-71.

35. Samstein RM, Lee C-H, Shoushtari AN, Hellmann MD, Shen R, Janjigian YY. Tumor mutational load predicts survival after immunotherapy across multiple cancer types. Nature genetics. 2019; 51(2): 202-6.

36. Leroy B, Anderson M, Soussi T. TP 53 mutations in human cancer: database reassessment and prospects for the next decade. Human mutation. 2014; 35(6): 672-88.

37. Li L, Li M, Wang X. Cancer type-dependent correlations between TP53 mutations and antitumor immunity. DNA repair. 2020; 88: 102785.

38. Jia Q, Wang J, He N, He J, Zhu B. Titin mutation associated with responsiveness to checkpoint blockades in solid tumors. JCI insight. 2019; 4(10).

39. Zhang X, Ma X, Wang Q, Kong Z. EZH2 targeting to improve the sensitivity of acquired radio-resistance bladder cancer cells. Transl Oncol. 2022; 16: 101316.